ACS Synthetic Biology

Research Article

pubs.acs.org/synthbio

Availability: A Metric for Nucleic Acid Strand Displacement Systems

Xiaoping Olson,[†] Shohei Kotani,[†] Jennifer E. Padilla,[†] Natalya Hallstrom,[†] Sara Goltry,[†] Jeunghoon Lee,[†,‡] Bernard Yurke,[†,§] William L. Hughes,*[,†] and Elton Graugnard*[,†]

[†]Micron School of Materials Science & Engineering, [‡]Department of Chemistry & Biochemistry, and [§]Department of Electrical & Computer Engineering, Boise State University, 1910 University Drive, Boise, Idaho 83725, United States

Supporting Information

ABSTRACT: DNA strand displacement systems have transformative potential in synthetic biology. While powerful examples have been reported in DNA nanotechnology, such systems are plagued by leakage, which limits network stability, sensitivity, and scalability. An approach to mitigate leakage in DNA nanotechnology, which is applicable to synthetic biology, is to introduce mismatches to complementary fuel sequences at key locations. However, this method overlooks nuances in the secondary structure of the fuel and substrate that impact the leakage reaction kinetics in strand displacement systems. In an effort to quantify the impact of secondary structure on leakage, we introduce the concepts of *availability* and *mutual availability* and demonstrate their utility for network analysis. Our approach exposes vulnerable locations on the substrate and quantifies the secondary structure of fuel strands. Using these concepts, a 4-fold reduction in leakage has been achieved. The result is a rational design process that efficiently suppresses leakage and provides new insight into dynamic nucleic acid networks.

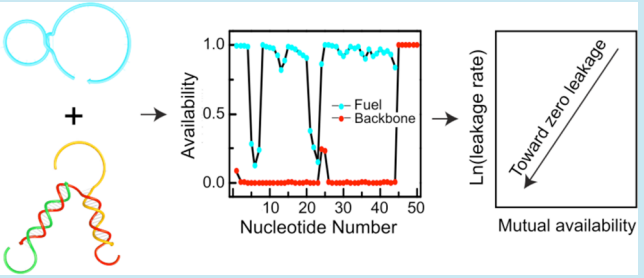

KEYWORDS: *nucleic acids, DNA, strand displacement, reaction networks, leakage, fraying, availability, mutual availability*

Nucleic acids are programmable materials because of their predictable Watson−Crick base pairing[1,2] and well-documented thermodynamics,[3−7] kinetics,[8−13] and mechanics.[14] In addition to static structures,[15−19] nucleic acids can be programmed into dynamic devices using toehold-mediated strand displacement,[9,20−22] whereby kinetic barriers to strand exchange are lowered via short complementary sequences that bring components into proximity. Dynamic nucleic acid technology utilizes toehold-mediated DNA strand displacement (DSD) to construct (1) nonenzymatic catalytic chemical reaction networks for isothermal signal amplification;[23−26] (2) catalytic hairpin assemblies for diagnostics, therapeutics, and theranostics;[27,28] (3) nanomachines[9,20,29] and walkers[30,31] for work and motility; (4) circuits for energy transport and logic;[32,33] and (5) networks for computation.[34−37] Although they are compelling, these demonstrations are limited in the scale and complexity necessary for real-world applications by a single fundamental challenge: *network leakage*. Leakage refers to the production of an unwanted output in the absence of an input, and it is the *Achilles' heel* of DSD systems, independent of the DNA/RNA system under consideration. The challenge of leakage must be overcome to achieve the device performance (i.e., speed, sensitivity, selectivity, stability, and scalabilty) necessary for broader adoption.

1.1. Leakage Problem. By design, DSD systems are metastable networks designed to be set into operation by the addition of a specific single-stranded sequence that triggers the reaction. Leakage occurs when system components react in the absence of a trigger, and its effect undermines the performance of catalytic networks,[24,38] seesaw gates,[36] catalytic hairpin assemblies,[26,39,40] and hybridization chain reactions.[25] Extrinsic sources of leakage, including chemical impurities, defective oligonucleotides, and malformed network components, can be minimized with careful processing.[26,41] In comparison, intrinsic leakage results from the design of the network, even if the components are perfect, and limits the ultimate DSD performance.

Sources of intrinsic leakage may be understood by considering the catalytic reaction network from Zhang et al. illustrated in Figure 1a.[24] In this representation, unique sequences are represented by labeled domains and complementary domains are denoted with asterisks (strand sequences are provided in Supporting Information S1). This network consists of a three-strand *substrate* complex in which the "upper" *signal* and *output* strands occupy domains of the lower *backbone* strand. Briefly, network operation is designed to be triggered by a single-stranded *catalyst* strand that hybridizes with an exposed backbone toehold (y*) and initiates three-way branch migration to displace the signal strand and expose a sequestered backbone toehold (3*). The catalytic cycle is completed by a similar process with the *fuel* strand reacting with the backbone to displace the output strand, the original catalyst, and form a *waste* product, as illustrated. As the end of a

Received: November 13, 2015
Published: February 15, 2016

DOI: 10.1021/acssynbio.5b00231
ACS Synth. Biol. 2017, 6, 84−93

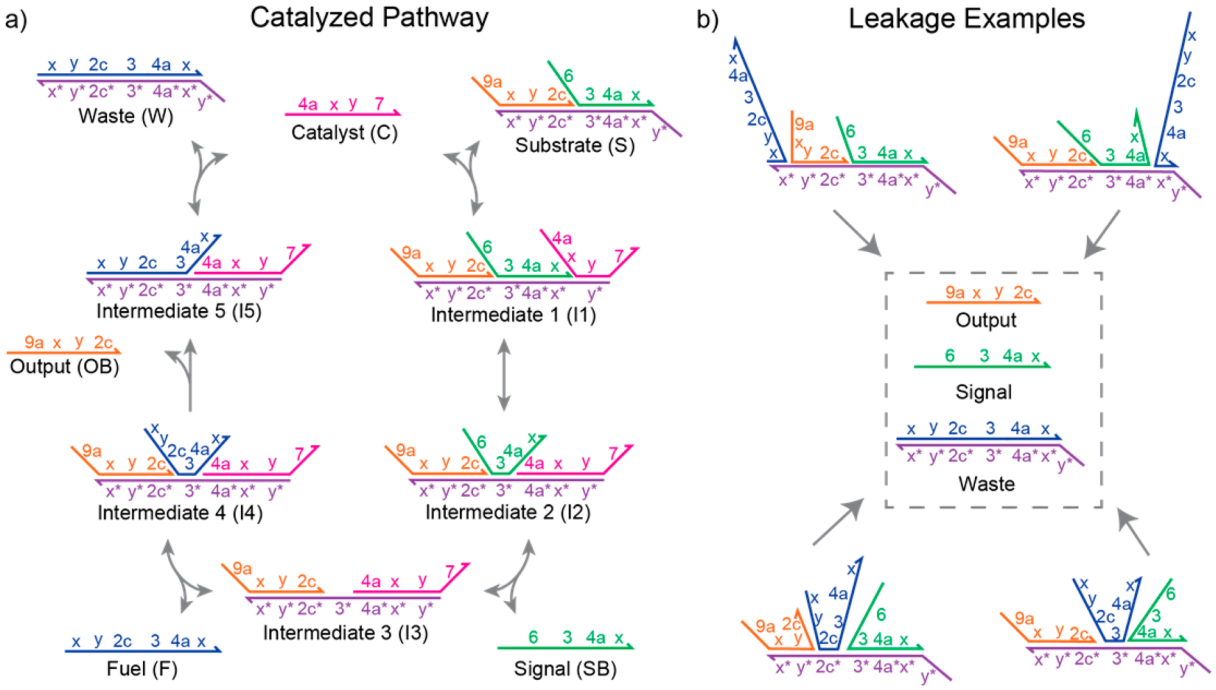

Figure 1. Domain representation of the catalytic DNA strand displacement system from Zhang et al.[24] and four example leakage pathways. (a) In the catalyzed strand displacement pathway of the reaction network, a catalyst strand initiates a reaction cycle driven forward thermodynamically by a net gain in entropy. The strand displacement exchanges the catalyst for the signal strand and exposes a sequestered toehold on the substrate backbone for the fuel, which reacts with the intermediate to complete the cycle and form a waste duplex. Sequences and domains are listed in Supporting Information S1. (b) In the four leakage pathways, the fuel reacts with the substrate backbone in the absence of a catalyst by exploiting fraying at the 5′, nick, and 3′ locations of the substrate.

cycle results in no gain or loss of base pairs, this network is driven forward thermodynamically by a net gain in entropy.

In this network, leakage occurs when the substrate and fuel react to produce signal in the absence of catalyst. This leakage reaction depends on successful nucleation of the fuel strand in the absence of an intended toehold. Fuel and substrate must bump into one another favorably, meaning that key bases must have some chance to interact and nucleate. Once nucleated, the leakage reaction proceeds through a branch migration process until strand invasion is complete. In this process, under the conditions reported here, nucleation is the rate-limiting step for the leakage reaction.[8,11,42] Example leakage reactions are shown in Figure 1b.

1.2. Thermal Fluctuations in DNA. Although often considered to be a zero toehold strand displacement event,[43] intrinsic leakage reactions are enabled by transient toeholds created via thermal fluctuations at the ends of the substrate and at the nick between the output and signal strands. *Breathing* refers to the spontaneous dissociation of individual base pairs in the interior of the duplex, and *fraying* is dissociation of the terminal base pairs (at the duplex ends or nicks). Studies of base pair fluctuations indicate that at room temperature the terminal base pairs are 50% open and the penultimate bases (one base pair from the ends of a duplex) are 10−20% open, whereas the fraction of open interior base pairs is $\sim 10^{-6}$ with an open lifetime of ~0.1 μs.[44−46] Additionally, single-stranded DNA overhangs (toeholds or specificity domains, such as domains y* and 9a in Figure 1a) increase the stability of the neighboring duplex base pairs, but they do not prevent fraying.[44] Thus, fraying of two base pairs at the ends and nick point of the substrate duplex is expected to be the dominant leakage mechanism. These vulnerable regions are highlighted in Figure 2a.

Leakage caused by fraying, when compared to toehold invasion, is approximately 4−6 orders of magnitude slower.[11] Even this small leakage drastically limits the scalability of feed-forward, cross-catalytic, and autocatalytic networks, where fuel invasion will unintentionally release the catalyst of the coupled networks. Thermal fluctuations such as fraying have long been suspected as the source of intrinsic leakage, and strategies to suppress it include (1) careful sequence and domain design such as using GC pairs at the fraying locations,[24] (2) use of proper reaction conditions,[47] (3) use of GC-rich sequences or introduction of buffer or clamping domains that are absent from fuel sequences,[36,40] (4) sequestration of domains in hairpin structures,[48] (5) use of extremely pure DNA strands made in bacteria,[26] (6) incorporation of mismatches,[39] and (7) novel domain level redundancy.[49] While each of these approaches has shown some effect, a clear set of design rules have not emerged for consistently and efficiently reducing leakage.

1.3. Insight from Secondary Structure. While previous studies have targeted the location and thermodynamic cost of mismatches in strand displacement systems,[39,50] design principles such as mismatch positions, mismatch numbers, and mismatch identities for suppressing leakage have not emerged. Importantly, base pair mismatch modifications also change the ensemble of DNA secondary structures, which can impact their nucleation and branch migration rates.[51,52] Here, we report a systematic investigation of the effects of mismatches on intrinsic leakage suppression and network performance using the network shown in Figure 1. All one and two base-pair mismatches produced by fuel strand sequence

DOI: 10.1021/acssynbio.5b00231
ACS Synth. Biol. 2017, 6, 84−93

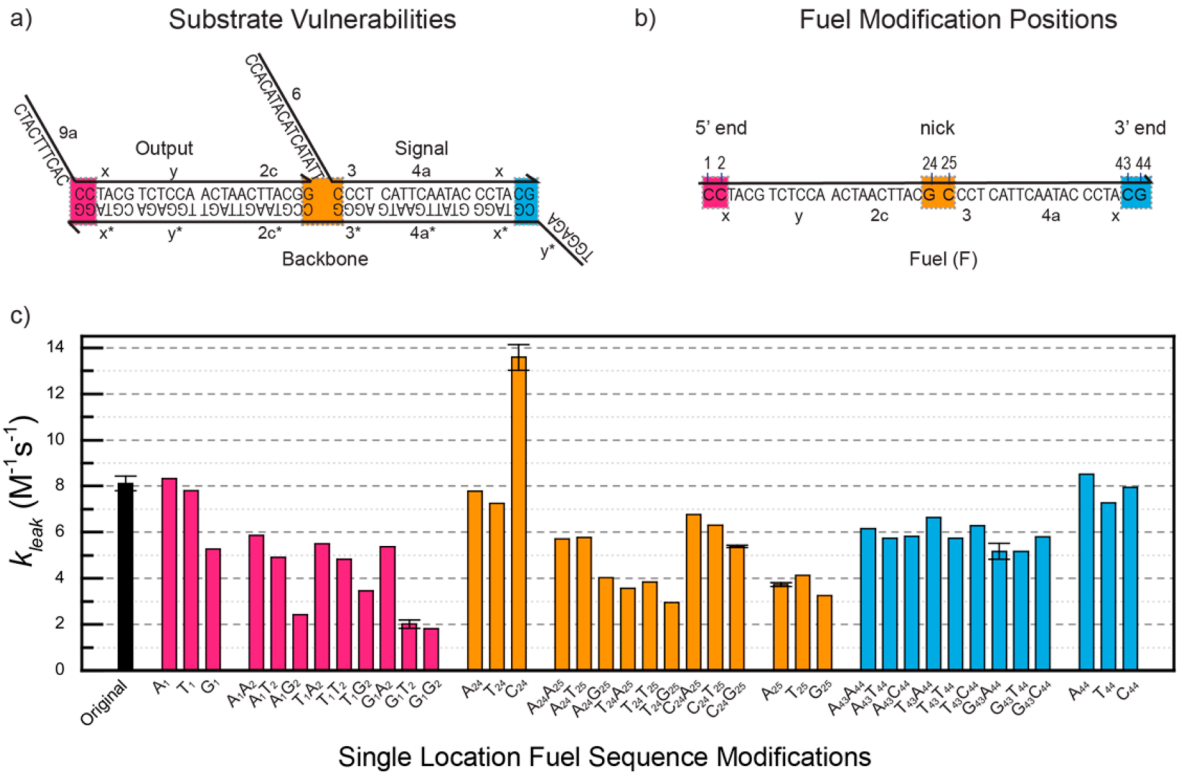

Figure 2. (a) Sequence and domain representation of the substrate with fraying locations highlighted. (b) Sequence and domain representation of the original fuel strand. Corresponding to the fraying locations of the substrate, the locations of fuel base mismatches are numbered, highlighted, and shown in bold font. They are 5′ end (bases 1 and 2), nick (bases 24 and 25), and 3′ end (bases 43 and 44). (c) Leakage rate constants for fuel modifications. The concentrations for leakage reactions are fuel (1300 nM), substrate (14 nM), and reporter (20 nM). The black bar represents the leakage rate with the original fuel strand. Pink, orange, and blue bars represent leakage rates for fuels with 1 and 2 nt modifications at 5′, nick, and 3′ locations, respectively. The rates are labeled by the identity of the modified base and its location on the fuel (see panel (b) for locations and originial base idenities). For example, G_1T_2 indicates that base 1 was changed from C to G and base 2 was changed to C to T. Error bars show the standard deviation from the mean for select samples in triplicate to estimate experimental error.

modifications were characterized at the 5′, 3′, and nick locations (see Figure 2a,b) by measuring the reaction rates of uncatalyzed (leakage) and catalyzed reactions using fluorescence photometry. These locations are related to locations on the substrate where fraying is expected to occur and enable nucleation between the backbone and fuel in the absence of catalyst. The results were analyzed on the basis of the mismatch identity, mismatch position, mismatch numbers, and the secondary structure of the fuel strands. To quantify the effects of secondary structure on leakage rates, we calculated the probability that a base is unpaired at equilibrium using NUPACK,[7,53] as discussed below. We define this probability as the *availability* of a base and introduce availability as a design concept for analyzing and engineering the stability of DNA reaction networks. To further understand the relationship between leakage rates and secondary structures, we define *total mutual availability* as the sum of all pairwise products of the availabilities of corresponding bases between fuels and the backbone. Taking consideration of both mismatches and secondary structure provides a more complete analysis of leakage suppression, and inclusion of the availability and mutual availability during our analysis provides insight toward rational design principles for minimizing leakage.

2. RESULTS AND DISCUSSION

2.1. Effect of Mismatch on Leakage Rate Constants. The leakage data for each fuel modification were fit with a second-order kinetics model to extract the leakage rate constant, k_{leak} (Supporting Information S3), and the results are shown in Figure 2c. The largest leakage suppression was observed for fuel modifications that created two mismatches at the 5′ end of the fuel (bases 1 and 2) and one or two mismatches at the nick in the substrate (base 25 and/or bases 24 and 25). While these locations showed consistent leakage suppression, no clear pattern between mismatch base identities and leakage rates emerged. For example, G−A and G−T mismatches show no suppression at base 1 and a factor of 2 suppression at base 25, whereas a G−G mismatch reduces leakage in both locations despite the fact that G−G mismatches have a lower energy penalty than other G or C mismatches when placed within a DNA duplex.[6] While the G−G mismatch consistently reduces leakage at bases 1, 2, and 25, no clear impact from mismatch identity is observed for bases 43 and 44. Although excess fuel in solution could interfere with leakage from the 3′ end of the fuel (at the toehold of the substrate backbone; see Supporting Information S4), the data indicates that mismatch identity alone or an associated energy penalty does not ensure leakage suppression.

2.2. Availability. Beyond mismatch identity, key insight into leakage suppression can be gained by analysis of the secondary structure ensembles of the original and modified fuels. While domain level designs assume the fuel to be purely single-stranded, thermodynamic analysis using NUPACK reveals a range of secondary structures. The minimum free energy (MFE) structures are shown in Figure 3a and have a

DOI: 10.1021/acssynbio.5b00231
ACS Synth. Biol. 2017, 6, 84−93

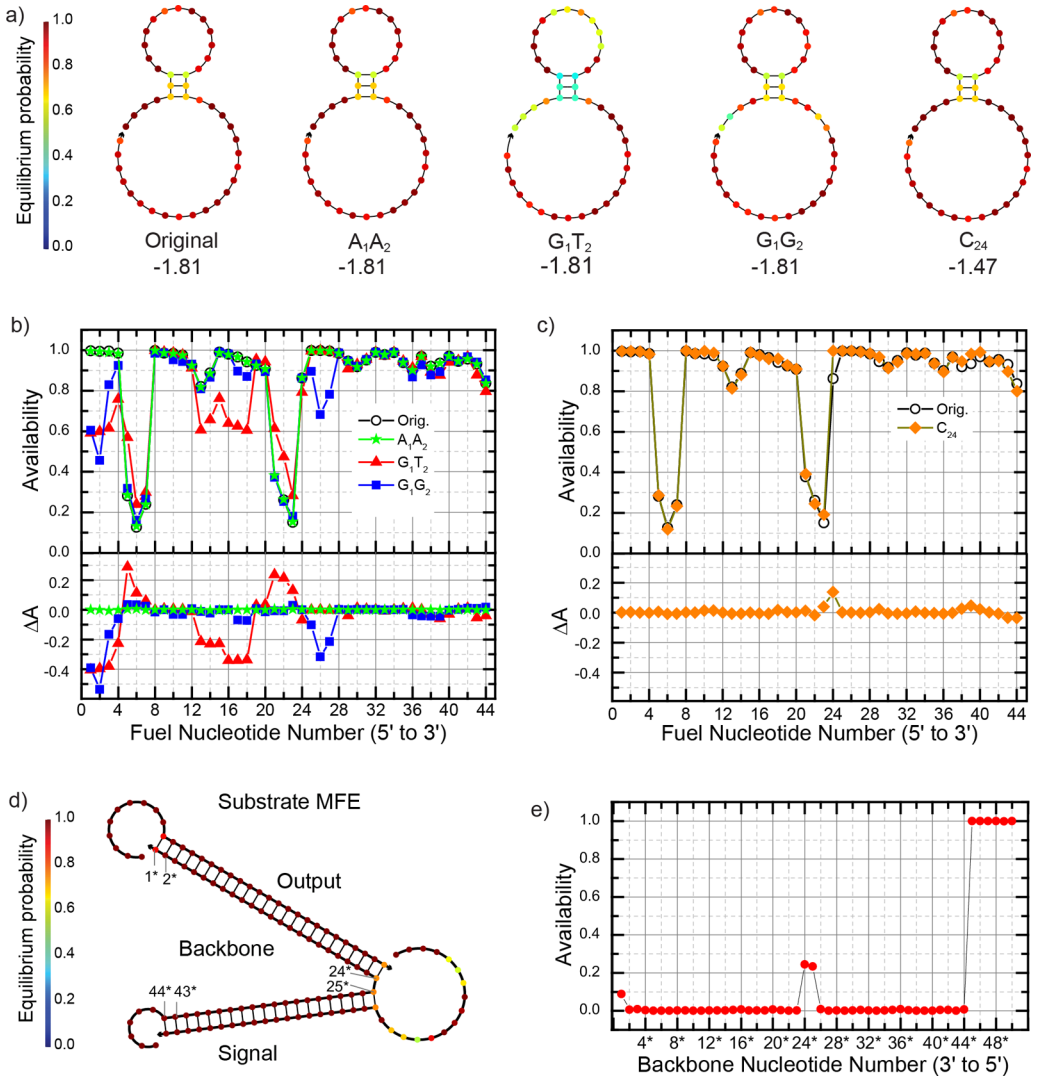

Figure 3. Minimum free energy (MFE) structures and base availabilities for select fuel strands and the substrate backbone. (a) MFE structures of the original fuel strand and fuel modifications A_1A_2, G_1T_2, G_1G_2, and C_{24} calculated by NUPACK. The Gibbs free energy of each structure is provided in units of kcal/mol. (b) Base availabilities for the original fuel and fuel modifications A_1A_2, G_1T_2, and G_1G_2 (upper plot) and the difference in base availabilities (ΔA) for each modification relative to the original fuel (lower plot). (c) Base availabilities for the original fuel and fuel modification C_{24} (upper plot) and the difference in availability relative to the original fuel (lower plot). (d) MFE structure of the substrate calculated by NUPACK. (e) Availability of each base in the backbone strand of the substrate. Because the fuel strand hybridizes with the backbone strand on the substrate, the base positions of the backbone strand were plotted on the *x* axis and labeled to correspond to the complement of the fuel strand.

moderate level of base pairing between six nucleotides of the fuels. Although the MFE structures indicate base pairing between bases 5−23, 6−22, and 7−21 for all but one (G_{25}) fuel sequence, the probability of pairing is affected by the modifications at bases 1, 2, 24, 25, 43, and 44. The MFE structures for all fuels are provided in Supporting Information S5. G_{25} indicates that base 25 was changed from C to G. More generally, the letter denotes the base identity and the number denotes the base position from 5′ end of the fuel. While the MFE structures are color-coded by the probability for being in the particular MFE structure shown, greater clarity is obtained by plotting the *availability* for each base in the fuel sequences, as shown in Figure 3b,c (upper plots). We define availability as the probability that a base is unpaired at equilibrium, and it quantifies the per-base effects of a sequence's ensemble of secondary structures. Availability is calculated by NUPACK from the predicted secondary structure ensemble lacking pseudoknots and non-Watson−Crick interactions.[7,53] Modifications to the fuel strand alter the availability of the bases since each sequence has a unique ensemble of secondary structures. Figure 3b,c (lower plots) shows the changes in base availabilities for modified fuel strands relative to the original fuel sequence. NUPACK calculations were performed using the following parameters: (1) 25 °C operating temperature; (2) 0.05 M Na^+ and 0.0115 M Mg^{2+} ion concentrations; (3) 14 nM substrate component concentrations, allowed complex size of 3; (4) 1.3 μM fuel concentration, allowed complex size of 2; and (5) dangles set to "all" in all cases to account for single-stranded tails.

Consistent with the MFE structures shown in Figure 3a, the availabilities of fuel bases 5, 6, 7, 21, 22, and 23 range between 0.1 and 0.6. However, several other bases have availabilities less than 1, which influences the probability of those bases nucleating a leakage reaction. Additionally, availability calculations exhibit subtle changes for modified fuel strands (Figure 3b,c) that have a large impact on leakage and are not limited to

DOI: 10.1021/acssynbio.5b00231
ACS Synth. Biol. 2017, 6, 84−93

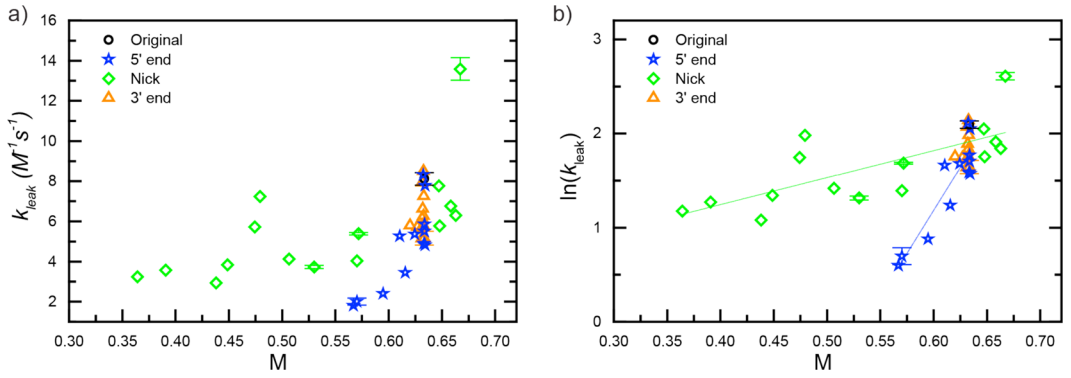

Figure 4. (a) Leakage rate constants for each fuel modification plotted versus total mutual availability between the fuel strand and the backbone strand on the substrate. The leakage rate for the original fuel is shown in black, while the 5′ end, nick and 3′ end fuel modifications are shown in blue, green, and orange, respectively. Representative error bars of select samples are shown, indicating that the scatter of the data is greater than the experimental error. Error bars represent the standard deviation of the mean of three samples. (b) Natural log plot of the leakage rate constant versus the total mutual availability. The green, and blue lines are the fits for the nick modifications, 5′ end modifications.

the modified bases. For example, the availabilities of several bases were considerably different between the original fuel and the G_1T_2 fuel (Figure 3b), especially for bases 1−4 and bases 13−18, which show a drop, and bases 21−23, which show a rise. While most modifications decreased availability for certain bases or left them nearly unchanged (for example, A_1A_2; Figure 3b), the C_{24} fuel modification increased the availability of several bases when compared to that of the original fuel (Figure 3c) and exhibited the highest leakage rate measured (Figure 2c). The base availabilities for all fuel modifications are provided in Supporting Information S6 and are ordered in terms of leakage rate in Figure S4. The data clearly show the positive correlation between lower fuel base availability and lower leakage rate.

To fully exploit the concept of availability for understanding the source of leakage, the availability of the bases of the substrate backbone must also be considered because both fuel and backbone bases must be available simultaneously for nucleation to occur. Figure 3d,e shows the MFE structure of the substrate and availability of the backbone bases. Ideally, the backbone would have zero availability within double-stranded domains (bases 1*−44*) and unity availability at the toehold (bases 45*−50*). However, the availabilities are ∼0.1 at base 1* ∼0.24 at base 24*, and ∼0.23 at base 25*, indicating that the substrate is vulnerable to leakage at these locations (i.e., nucleation with bases 1, 24, and/or 25 of the fuel strands). Thus, in the context of the substrate, availability quantifies the degree of fraying or breathing of the duplex bases.

2.2.1. Base Modifications at the 5′ End of the Fuel. Given that bases 1*, 24*, and 25* of the substrate backbone are most vulnerable to leakage, fuel modifications that reduce availability for fuel bases 1, 24, and 25 can be expected to exhibit the lowest leakage, and this is shown to be the case. For example, leakage was suppressed for the G_1, G_1T_2, and G_1G_2 fuel modifications. The G_1 leakage drop corresponds to a 5% reduction in the availability of bases 1 and 2 (Supporting Information S6). In addition, the availability of bases 1 and 2 of G_1T_2 decreased 40%, whereas for G_1G_2, the availability of bases 1 and 2 decreased 40 and 54%, respectively (Figure 3b). These modified fuels yielded a 4-fold reduction in leakage when compared to that of the original fuel strand. In contrast, the base availabilities in A_1, T_1, and A_1A_2 strands are nearly identical to the original fuel strand (Figure 3b and Supporting Information S6), and their leakage suppression was minimal. Here, the changes in availability for single bases on the modified fuel strands provide a compelling explanation for the variation in leakage rates.

2.2.2. Base Modifications at the 3′ End of the Fuel. The low availabilities at backbone bases 43* and 44* imply a lack of fraying, which would be expected to minimize the impact of changes in the availabilities of fuel bases 43 and 44 at the 3′ end of the fuels. This hypothesis is consistent with the uniform and relatively minor leakage reductions for fuels with reduced availabilities at bases 43 and 44, such as $T_{43}T_{44}$ and $G_{43}T_{44}$ (Supporting Information S6). However, the data for leakage at bases 43* and 44* are confounded by spurious hybridization of the fuel's y domain with the y* toehold domain of the substrate (bases 45* to 50*). This hybridization causes the x domain of both the fuel strand and the signal strand to compete to bind with the x* domain of the substrate (Supporting Information S4). The competition is expected to be significant since the fuel is at 100× excess concentration. This spurious hybridization is expected to sterically hinder leakage at bases 43* and 44* of the backbone and is likely an important factor in the lack of variation in the leakage rate for base modifications at the 3′ end of the fuel strand.

2.2.3. Base Modifications of the Fuel at the Nick Location. Base 24* and base 25* on the substrate backbone have high availabilities, which suggests a greater degree of fraying (Figure 3e). Consistent with this expectation, all fuel mismatch modifications at base 25 were observed to suppress the leakage rates. We attribute the reduced leakage for mismatch modifications at fuel base 25 to the lower availabilities at base 25 for the modified fuels compared with the original fuel. For example, availabilities at base 25 for A_{25}, T_{25} and G_{25} were reduced from 21% to 62% and the leakage was reduced from 49% to 68% compared with original fuel. A similar correlation between availability and leakage rate was observed for mismatch modifications at fuel base 24. The single base mismatch at fuel base 24 reduced the leakage for T_{24}, for which the availability of base 24 decreased by 72%. The leakage nearly doubled for C_{24}, which exhibited a 16% higher availability for base 24. Lastly, no change in leakage rate was observed for A_{24}, for which the base 24 availability increased by 9%. An additional factor in the increased leakage observed for C_{24} may stem from its increased availability at several bases when compared to the original sequence (Figure 3c). An increase in availability corresponds to a decrease in secondary structure, which then lowers the

DOI: 10.1021/acssynbio.5b00231
ACS Synth. Biol. 2017, 6, 84−93

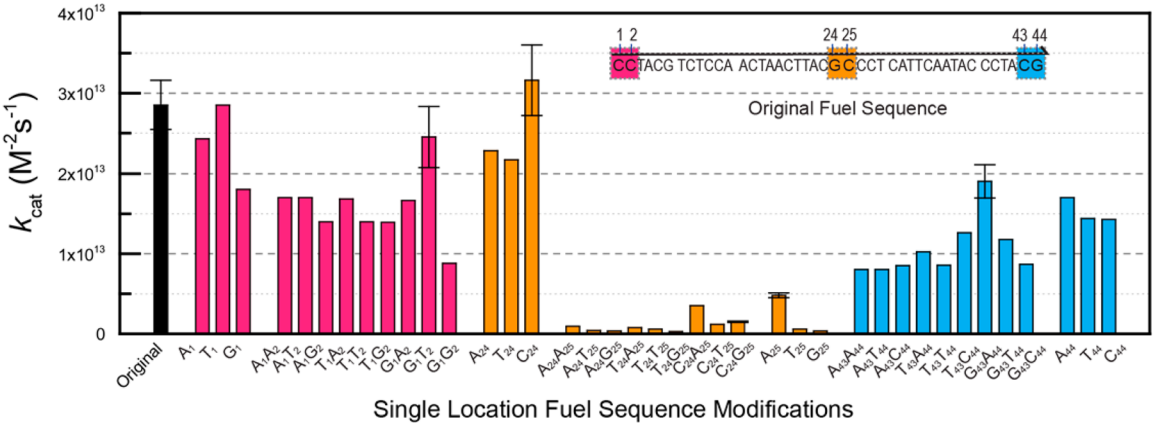

Figure 5. Rate constants of catalyzed reactions between the catalyst (1 nM), fuel (13 nM), substrate (14 nM), and reporter (20 nM) monitored via fluorescence. The black bar represents the original fuel strand. Pink, orange, and blue bars represent 1 and 2 nt modifications at 5′, nick, and 3′ locations, respectively. Error bars show the standard deviation from the mean for select samples in triplicate to estimate experimental error.

activation energy for nucleation between fuel and substrate. For further consideration, an analysis of base availability in the context of the intuitive energy landscape model of Srinivas et al.[11] is provided in Supporting Information S7.

2.3. Mutual Availability. On the basis of the above observations, base availability is a potentially powerful new design tool with base-specific resolution. In our qualitative explanations, we focused on the separate availabilities of the bases of the fuel or substrate backbone strands. However, as noted above, leakage reactions require nucleation of these strands with each other. To analyze the combined effects of the availabilities of bases from both strands and to find a quantifiable correlation, we define and analyze a *mutual availability* (m_{ij}) and *total mutual availability* (M). The mutual availability is simply the product of the availabilities of any two bases, defined as $m_{ij} = P_{F(i)}P_{B(j)}$, where $P_{F(i)}$ is the availability of base i of the fuel strand and $P_{B(j)}$ is the availability of base j of the backbone strand within the substrate complex. The total mutual availability is defined as $M = \sum_i(m_{ii^*}) = \sum_i(P_{F(i)}P_{B(i^*)})$, where i indexes the complementary base pairs in the fuel-substrate waste product in correct registration. In other words, i^* is the base position of backbone strand that matches the complementary position i of the fuel strand.

For nucleation to occur, key bases of the fuel and backbone must be available to hybridize. Total mutual availability, M, as defined above, provides a quantitative metric for analyzing fuel and substrate sequence interactions. To assess whether M could be correlated with leakage rate, Figure 4a plots leakage rates versus the calculated values of M for all fuel sequence modifications. On the basis of the apparent exponential dependence, the natural log of the leakage rate constant is plotted versus M in Figure 4b and is colored-coded by 5′, 3′, and nick modifications of the fuel. Select experiments were repeated in triplicate, and the scatter of the data is greater than the experimental error. Error bars represent the standard deviation of the mean.

Linear fits to the data are provided as guides to the eye. The 5′ and nick modifications exhibited linear trends and were fit individually. Given the near zero availability of base 44* of the backbone, 3′ fuel modifications had very little impact on total mutual availability. The nick fuel modifications and their corresponding fit are depicted in green and have a slope of 2.87 with an adjusted R^2 value of 0.50. 5′ fuel modifications and their corresponding fit are depicted in blue and have a slope of 18.26 with an adjusted R^2 of 0.81. While the primary discussion here is focused on single location fuel modifications, multiple location modifications (e.g., 5′ end *and* nick locations) further reduced the leakage rate to an almost undetectable level (about 100-fold), which are presented and discussed in Supporting Information S8. These data provide further support for total mutual availability as a metric for leakage.

The leakage rate constant appears to be exponentially related to the total mutual availability of the fuel and substrate backbone, suggesting that M may be related to a nucleation activation energy barrier. However, our data do not distinguish between barriers to nucleation and branch migration nor can they identify the critical nucleus for leakage to proceed. The scatter in Figure 4 may result from the incompleteness of our mutual availability model, which does not include branch migration steps, and limitations in total mutual availability as a measure of nucleation barriers. For example, NUPACK does not include pseudoknots, G-quartets, nick overhangs, and the coaxial stacking parameter into its calculations. Additionally, base availability, as defined, does not include tertiary nucleic acid structure. The correlation between the leakage rate constant and total mutual availability also needs careful consideration. For example, as the number of fuel mismatches increases, the leakage rate approaches zero, and the reaction stalls because of a lack of thermodynamic driving force. In comparison, when the total mutual availability is high, an effective toehold is formed, and the nucleation barrier is reduced, which means diffusion is the rate-limiting factor. The relationship between M and the leakage rate constant is thus constrained by these limits.

2.4. Catalyzed Reactions. It has generally been observed that the rate constants between catalytic reactions and leakage reactions are coupled. It has been shown that when leakage rates were reduced by introducing mismatches, catalytic rates were also decreased or maintained.[39] Likewise, here we also found that some fuel mismatch modifications maintained the original catalytic rate while decreasing the leakage rates. The kinetics data of each fuel modification were fit with a third-order kinetics model with an approximation to extract the catalyzed rate constant, k_{cat} (Supporting Information S3). Catalyzed rate constants ranged 3 orders of magnitude for the fuel modifications and are plotted in Figure 5.

The effect of fuel sequence modifications on the catalyzed reaction can be understood via the reaction mechanism. The

DOI: 10.1021/acssynbio.5b00231
ACS Synth. Biol. 2017, 6, 84−93

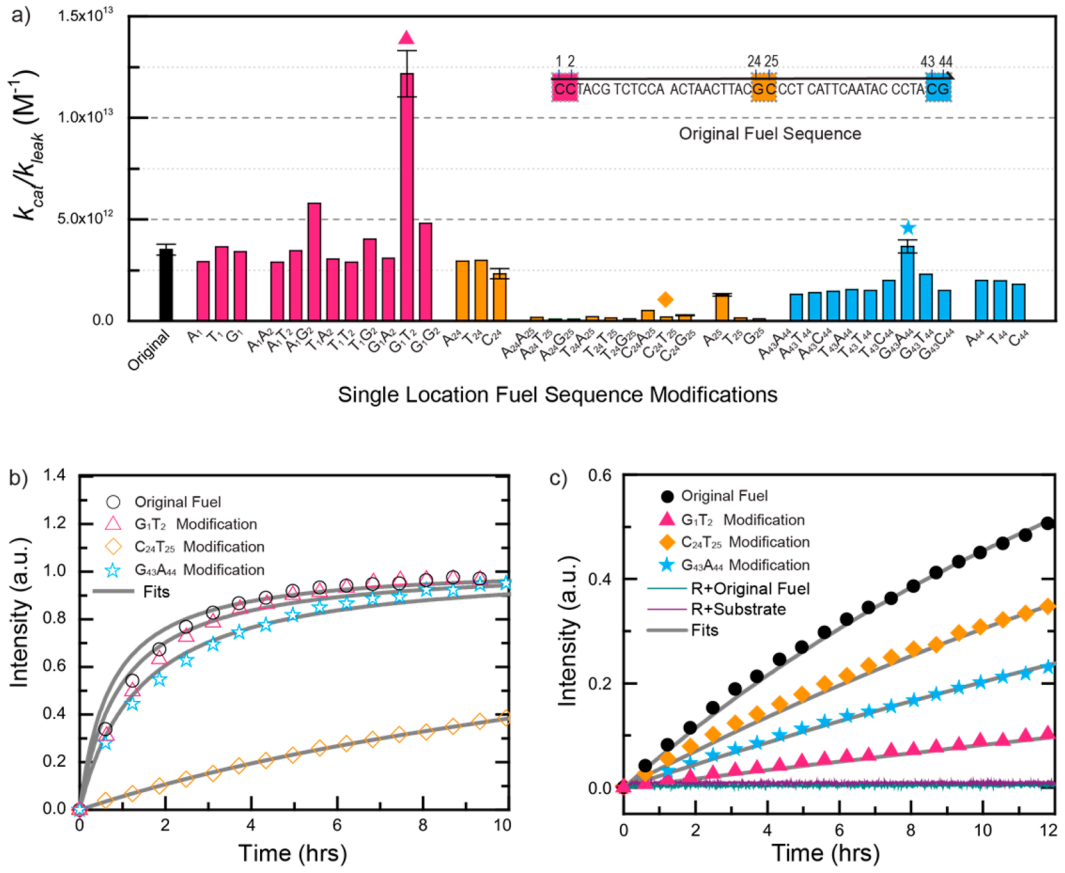

Figure 6. (a) Ratio of the catalyzed to leakage reaction rates (k_{cat}/k_{leak}) for single location fuel modifications to evaluate overall system performance. Catalyzed reactions were performed with the catalyst (1 nM), fuel (13 nM), substrate (14 nM), and reporter (20 nM), monitored via fluorescence, and uncatalyzed leakage reactions were performed with fuel (1300 nM), substrate (14 nM), and reporter (20 nM). The black bar represents the original fuel strand. Pink, orange, and blue bars represent 1 and 2 nt modifications at 5′, nick, and 3′ locations, respectively. Error bars show the standard deviation from the mean for select samples in triplicate to estimate experimental error. (b) Representative fluorescence data of catalytic reactions: the original fuel (empty black circles), G_1T_2 modified fuel (empty red triangles), $C_{24}T_{25}$ modified fuel (yellow diamonds), and $G_{43}A_{44}$ modified fuel (empty blue stars). (c) Representative fluorescence data of leakage reactions: the original fuel (solid black circles), G_1T_2 modified fuel (solid red triangles), $C_{24}T_{25}$ modified fuel (solid yellow diamonds), and $G_{43}A_{44}$ modified fuel (solid blue stars). The gray lines are the calculated fits to each curve, and the solid blue and purple lines represent reactions between the reporter and the original fuel and the reporter and the substrate, respectively.

modification positions play a critical role in the catalyzed reaction, as discussed further in Supporting Information S8 and S9. In Figure 5, trends can be observed by grouping the modification positions of the fuel strand at the 5′ end (bases 1 and 2) with base 24 of the nick and at the 3′ end (bases 43 and 44) with base 25 of the nick. As expected from the reaction mechanism shown in Figure 1, mismatches at base 25 of the nick location have the greatest impact because it affects fuel hybridization with the intermediate (I3), followed by mismatches at the 3′ end that impede catalyst release. Fuel modifications at the 5′ end and base 24 of the nick locations have minimal impact on the catalytic rate. A strategy to speed up the catalytic reaction is to increase the fuel toehold length by deleting one nucleotide at the 5′ end of the catalyst. Preliminary experiments for multiple-location fuel modifications indicate that this approach is effective for fuels that include a modification at base 25, whereas it has a counter effect for other fuel modifications (Table S1 and Supporting Information S8).

Since one catalytic reaction cycle in this system has many intermediate steps including toehold exchange, toehold-mediated strand displacement, and spontaneous toehold dissociation, the correlation between the overall catalytic rate constant and the total mutual availability of the catalyzed reaction was not studied in this work.

2.5. System Performance. An ideal DNA strand displacement system would have elevated selectivity to the catalyst, sensitivity to the catalyst, high catalytic turnover (high k_{cat}), stability in the absence of the catalyst (low k_{leak}), and scalability because of suppressed crosstalk and leakage. Thus, as a practical metric for the performance of the system, we use the ratio, k_{cat}/k_{leak}. The larger the ratio, the greater will be the capacity to distinguish a response to the catalyst from the background leakage.

Given that the leakage rate is strongly coupled to the catalytic rate for fuel sequence modifications at bases 25, 43, and 44, the suppression of the catalytic reaction reduced performance more than leakage suppression increased it. Locations of strong coupling between catalytic rate and leakage rate can be considered to be limitations of intrinsic leakage suppression; they are a result of the domain design of this system and will be different for other domain level designs. Modifications at base 24 had no net benefit due to the low availability of the substrate at this location. Improvements in performance came from

DOI: 10.1021/acssynbio.5b00231
ACS Synth. Biol. 2017, 6, 84−93

introducing sequence mismatches at the 5′ end of the fuel (bases 1 and 2), where leakage and catalytic reaction rates are decoupled. As measured by the k_{cat}/k_{leak} ratio, the G_1T_2 fuel modification has the best performance overall (Supporting Information S10). This modification targeted the vulnerability at base 1* of the backbone strand due to nonzero availability. It reduced the leakage reaction rate by a factor of 4 but maintained a catalytic rate close to the original fuel strand (Figure 6a).

In the literature, mismatch modifications have shown more dramatic improvements to leaky systems and systems using low-quality strands. Mismatches in Jiang et al.'s DNA catalytic hairpin design with large leakage showed 25-fold improvements in signal-to-background ratio compared with that of the original hairpins.[39] By contrast, Bhadra et al.'s optimized RNA catalytic hairpin system shows only 7-fold leakage reduction, without disturbing the catalytic reaction rate, by introducing mismatch modifications. However, when using unpurified RNA strands in this system, a 13−15-fold reduction in the leakage is observed when compared to that of the control.[54] Zhang et al.'s system was optimized and purified, having an intrinsic leakage rate of only ∼8 M^{-1} s^{-1}. This work demonstrates that a 4-fold leakage reduction in this system can be achieved while leaving the catalyzed reaction rate nearly unchanged. Mismatches at substrate fraying locations reveal the power of availability to influence circuit performance.

2.6. Availability Analysis of Other Networks. The concept of mutual availability is expected to apply to other network designs as well. In an effort to validate the mutual availability concept with another network design, we analyzed a hairpin design from Jiang et al.[39] Their study provided sufficient data to apply an analysis of total mutual availability, and we estimated the rate constants for the hairpin design, as described in Supporting Information S11. Even though the total mutual availability values vary relative to the Zhang et al. network, the observed trend is the same, even in a different buffer. The results provide compelling support for the validity of mutual availability as a metric for sequence-level network analysis and design.

2.7. Conclusions. The effects of base-pair mismatches on leakage suppression and total network performance were systematically investigated using the well-established catalytic reaction network from Zhang et al.[24] Fuel modifications at the 5′, 3′, and nick locations were chosen because they correspond to vulnerable substrate locations where nucleation is expected to occur. Qualitatively, availabilities of the substrate and the fuel strand bases were found to correspond well to observed trends in the leakage rate data. Quantitatively, a trend between the total mutual availability and the leakage rates was observed regardless of mismatch identities, mismatch numbers, and mismatch locations. This work suggests availability and mutual availability as design concepts for optimal performance of nucleic acid reaction networks.

Future work can further explore the correlation between the total mutual availability and the activation energy, aiming at a more detailed model of leakage mechanisms. In addition, the correlation between the overall catalytic rate constant (k_{cat}) and the total mutual availability of the catalyzed reaction should be studied to allow predictions of the practical metric for the performance of the system (k_{cat}/k_{leak}). This study also leaves room for refinement against other interactions that NUPACK does not calculate, such as G-quartets, non-Watson−Crick interactions, pseudoknots, and geometric constraints. With improved design metrics and refined design tools, non-enzymatic amplification systems can be used as amplifiers for diagnostics, and nucleic acid chemical reaction networks will become more robust tools for theranostics, molecular computation, and synthetic biology.

3. METHODS

3.1. Chemicals and DNA Complex Purification. Solvents and chemicals were purchased from Sigma-Aldrich unless otherwise noted. DNA oligonucleotides were synthesized and purified with high-performance liquid chromatography by Integrated DNA Technologies (IDT). Reporter strands were labeled with 5′ fluorophores (TET) and 3′ Iowa Black dark quenchers (IABkFQ) by IDT. Oligonucleotides were prepared in 1× TE buffer (10 mM Tris-HCl, pH 8.0, 1 mM EDTA, diluted from 100× TE). Final stock concentrations (100 μM) were confirmed by measuring the 260 nm absorbance (Eppendorf Biophotometer) using extinction coefficients provided by IDT.

TAE buffer (10×; 40 mM Tris, 40 mM acetate, 1 mM EDTA) was purchased from Hoefer or Fisher Scientific and then mixed with 125 mM $Mg(C_2H_3O_2)_2{\cdot}4H_2O$. DNA components were diluted to 30 μM in 1× TAE buffer with 12.5 mM Mg^{2+}. DNA components were annealed at 95 °C for 5 min using a thermocycler (Eppendorf Mastercycler Nexus Gradient) and cooled to room temperature over ∼90 min to form substrates and reporters.

Substrate and reporter complexes were purified by native polyacrylamide gel electrophoresis (N-PAGE). To eliminate malformed substrates, fuel and substrate were stoichiometrically incubated at 15 μM for 1 h at room temperature before loading the gel. The loading buffer contained a 1:1 ratio of bromophenol blue dye and ficoll solution (type 400, 20% water). Substrates were purified by N-PAGE in 14% acrylamide gels (made from 30% acrylamide/bis-acrylamide solution in a 29:1 ratio), which were run at 150 V for 7 h. Reporters were also purified by N-PAGE in 10% acrylamide gels, which were run at 150 V for 2 h. For both processes, the cooling system (VWR International) was set to 20 °C.

The bands of interest were cut out of the gels and eluted in 1× TE/Mg^{2+} buffer for 2 days at 4 °C. The buffer included 1× TE with 12.5 mM $MgCl_2{\cdot}4H_2O$ (Acros Organics) added.

Because Mg^{2+} binds to EDTA, the effective Mg^{2+} concentration was estimated to be 11.5 mM.[24] Substrate and reporter concentrations were quantified via measuring absorbance at 260 nm and calculated using extinction coefficients predicted by nearest-neighbor models (Supporting Information S2).[36,55] Typical yields were 30% for the substrate and 50% for the reporter.

3.2. Spectrofluorimetry. All experiments were carried out in 1× TE/Mg^{2+} buffer with a total volume of 1 mL in 4 mL disposable methacrylate cuvettes (Fisher Scientific) at 25 °C. DNA stock solutions were normally diluted to 2 μM before being added to each sample. A poly-T strand (dT_{20}) was added into all dilute stock samples (1 μM and lower) to reach a final concentration of 1 μM and prevent DNA loss via nonspecific binding to the microfuge tubes and pipet tips.[24] All solutions were gently mixed by pipetting.

Fluorescence intensity versus time was measured via fluorescence spectrophotometers (Agilent Technologies, Cary Eclipse). Sample solutions were excited at 510 nm, and the emission was measured at 538 nm. Slit sizes used were 2.5 nm for excitation and 10 nm for emission. Fluorescence was

DOI: 10.1021/acssynbio.5b00231
ACS Synth. Biol. 2017, 6, 84−93

normalized so that 1 normalized unit (a.u.) of fluorescence corresponded to 14 nM (the substrate concentration) for leakage reactions and 13 nM (the fuel concentration) for catalyzed reactions.

3.3. Reaction Measurements. For leakage reactions, the fluorescence intensity was continuously monitored for the first 12 h (shown in Figure 6c) with the samples maintained at 25 °C and then periodically measured until the reaction reached completion at room temperature (~21.5 °C). Substrate (14 nM) and reporter (20 nM) were reacted with ~100-fold excess of the fuel strands (1300 nM) to expedite leakage reactions and to extract intrinsic leakage specific to fuel and substrate interaction. Reaction between substrate and reporter was undetectable under this condition (Figure 6c). With the assumption that extrinsic leakage dominates at shorter times and intrinsic leakage dominates at longer times,[26] leakage was measured over the long term to extract intrinsic effects. For catalyzed reactions, the catalyst (1 nM), fuel (13 nM), substrate (14 nM), and reporter (20 nM) were reacted for 10 h (Figure 6b). During the experiments, substrate reactions were inferred by monitoring the production of signal strand through its reaction with the reporter (Supporting Information S1).

■ ASSOCIATED CONTENT

Supporting Information

The Supporting Information is available free of charge on the ACS Publications website at DOI: 10.1021/acssynbio.5b00231.

Strand sequences, additional schematics, equations, data on multilocation fuel modifications, availability and numerical data for all fuel strands, and further analysis of the catalyzed reactions rates (PDF)

■ AUTHOR INFORMATION

Corresponding Authors

*(W.L.H.) E-mail: willhughes@boisestate.edu.
*(E.G.) E-mail: eltongraugnard@boisestate.edu.

Author Contributions

The manuscript was written through contributions of all authors. All authors have given approval to the final version of the manuscript.

Notes

The authors declare no competing financial interest.

■ ACKNOWLEDGMENTS

This project was supported in part by (1) The W.M. Keck Foundation, (2) NIH Grant No. K25GM093233 from the National Institute of General Medical Sciences, (3) NIH Grant No. P20 RR016454 from the INBRE Program of the National Center for Research Resources, and (4) The Micron Foundation. We also thank the Nanoscale Materials & Device Research Group (nano.boisestate.edu) for valuable discussions.

■ REFERENCES

(1) Watson, J. D., and Crick, F. H. C. (1953) Molecular Structure of Nucleic Acids - a Structure for Deoxyribose Nucleic Acid. *Nature 171*, 737−738.

(2) Kool, E. T. (2001) Hydrogen bonding, base stacking, and steric effects in dna replication. *Annu. Rev. Biophys. Biomol. Struct. 30*, 1−22.

(3) Lu, M., Guo, Q., Marky, L. A., Seeman, N. C., and Kallenbach, N. R. (1992) Thermodynamics of DNA Branching. *J. Mol. Biol. 223*, 781−789.

(4) SantaLucia, J., Allawi, H. T., and Seneviratne, A. (1996) Improved nearest-neighbor parameters for predicting DNA duplex stability. *Biochemistry 35*, 3555−3562.

(5) SantaLucia, J. (1998) A unified view of polymer, dumbbell, and oligonucleotide DNA nearest-neighbor thermodynamics. *Proc. Natl. Acad. Sci. U. S. A. 95*, 1460−1465.

(6) SantaLucia, J., Jr., and Hicks, D. (2004) The thermodynamics of DNA structural motifs. *Annu. Rev. Biophys. Biomol. Struct. 33*, 415−440.

(7) Dirks, R. M., Bois, J. S., Schaeffer, J. M., Winfree, E., and Pierce, N. A. (2007) Thermodynamic analysis of interacting nucleic acid strands. *SIAM Rev. 49*, 65−88.

(8) Zhang, D. Y., and Winfree, E. (2009) Control of DNA Strand Displacement Kinetics Using Toehold Exchange. *J. Am. Chem. Soc. 131*, 17303−17314.

(9) Yurke, B., and Mills, A. (2003) Using DNA to Power Nanostructures. *Genetic Programming and Evolvable Machines 4*, 111−122.

(10) Panyutin, I. G., and Hsieh, P. (1994) The kinetics of spontaneous DNA branch migration. *Proc. Natl. Acad. Sci. U. S. A. 91*, 2021−2025.

(11) Srinivas, N., Ouldridge, T. E., Sulc, P., Schaeffer, J. M., Yurke, B., Louis, A. A., Doye, J. P. K., and Winfree, E. (2013) On the biophysics and kinetics of toehold-mediated DNA strand displacement. *Nucleic Acids Res. 41*, 10641−10658.

(12) Sikora, J. R., Rauzan, B., Stegemann, R., and Deckert, A. (2013) Modeling Stopped-Flow Data for Nucleic Acid Duplex Formation Reactions: The Importance of Off-Path Intermediates. *J. Phys. Chem. B 117*, 8966−8976.

(13) Graugnard, E., Cox, A., Lee, J., Jorcyk, C., Yurke, B., and Hughes, W. L. (2010) Kinetics of DNA and RNA Hybridization in Serum and Serum-SDS. *IEEE Trans. Nanotechnol. 9*, 603−609.

(14) Hagerman, K. R., and Hagerman, P. J. (1996) Helix rigidity of DNA: The meroduplex as an experimental paradigm. *J. Mol. Biol. 260*, 207−223.

(15) Seeman, N. C. (2010) Nanomaterials Based on DNA. *Annu. Rev. Biochem. 79*, 65−87.

(16) Linko, V., and Dietz, H. (2013) The enabled state of DNA nanotechnology. *Curr. Opin. Biotechnol. 24*, 555−561.

(17) Edwards, A., and Yan, H. (2014) DNA Origami. *Nucleic Acids Mol. Biol. 29*, 93−134.

(18) Endo, M., Yang, Y., and Sugiyama, H. (2013) DNA origami technology for biomaterials applications. *Biomater. Sci. 1*, 347−360.

(19) Saccà, B., Sprengel, A., and Feldkamp, U. (2013) De Novo Design of Nucleic Acid Structures, In *De Novo Molecular Design* (Schneider, G., Ed.) pp 495−517, Wiley-VCH, Weinheim, Germany.

(20) Yurke, B., Turberfield, A. J., Mills, A. P., Simmel, F. C., and Neumann, J. L. (2000) A DNA-fuelled molecular machine made of DNA. *Nature 406*, 605−608.

(21) Wang, F., Lu, C. H., and Willner, I. (2014) From Cascaded Catalytic Nucleic Acids to Enzyme-DNA Nanostructures: Controlling Reactivity, Sensing, Logic Operations, and Assembly of Complex Structures. *Chem. Rev. 114*, 2881−2941.

(22) Zhang, D. Y., and Seelig, G. (2011) Dynamic DNA nanotechnology using strand-displacement reactions. *Nat. Chem. 3*, 103−113.

(23) Bi, S., Zhang, J., Hao, S., Ding, C., and Zhang, S. (2011) Exponential amplification for chemiluminescence resonance energy transfer detection of microRNA in real samples based on a cross-catalyst strand-displacement network. *Anal. Chem. 83* (10), 3696−3702.

(24) Zhang, D. Y., Turberfield, A. J., Yurke, B., and Winfree, E. (2007) Engineering entropy-driven reactions and networks catalyzed by DNA. *Science 318*, 1121−1125.

(25) Dirks, R. M., and Pierce, N. A. (2004) Triggered amplification by hybridization chain reaction. *Proc. Natl. Acad. Sci. U. S. A. 101*, 15275−15278.

DOI: 10.1021/acssynbio.5b00231
ACS Synth. Biol. 2017, 6, 84−93

(26) Chen, X., Briggs, N., McLain, J. R., and Ellington, A. D. (2013) Stacking nonenzymatic circuits for high signal gain. *Proc. Natl. Acad. Sci. U. S. A. 110*, 5386−5391.
(27) Huttanus, H. M., Graugnard, E., Yurke, B., Knowlton, W. B., Kuang, W., Hughes, W. L., and Lee, J. (2013) Enhanced DNA sensing via catalytic aggregation of gold nanoparticles. *Biosens. Bioelectron. 50*, 382−386.
(28) Jung, C., and Ellington, A. D. (2014) Diagnostic Applications of Nucleic Acid Circuits. *Acc. Chem. Res. 47*, 1825−1835.
(29) Goltry, S., Hallstrom, N., Clark, T., Kuang, W., Lee, J., Jorcyk, C., Knowlton, W. B., Yurke, B., Hughes, W. L., and Graugnard, E. (2015) DNA topology influences molecular machine lifetime in human serum. *Nanoscale 7*, 10382−10390.
(30) Shin, J.-S., and Pierce, N. A. (2004) A Synthetic DNA Walker for Molecular Transport. *J. Am. Chem. Soc. 126*, 10834−10835.
(31) Yin, P., Yan, H., Daniell, X. G., Turberfield, A. J., and Reif, J. H. (2004) A Unidirectional DNA Walker That Moves Autonomously along a Track. *Angew. Chem., Int. Ed. 43*, 4906−4911.
(32) Cannon, B. L., Kellis, D. L., Davis, P. H., Lee, J., Kuang, W., Hughes, W. L., Graugnard, E., Yurke, B., and Knowlton, W. B. (2015) Excitonic AND Logic Gates on DNA Brick Nanobreadboards. *ACS Photonics 2*, 398−404.
(33) Graugnard, E., Kellis, D. L., Bui, H., Barnes, S., Kuang, W., Lee, J., Hughes, W. L., Knowlton, W. B., and Yurke, B. (2012) DNA-Controlled Excitonic Switches. *Nano Lett. 12*, 2117−2122.
(34) Benenson, Y. (2012) Biomolecular computing systems: principles, progress and potential. *Nat. Rev. Genet. 13*, 455−468.
(35) Qian, L., Winfree, E., and Bruck, J. (2011) Neural network computation with DNA strand displacement cascades. *Nature 475*, 368−372.
(36) Qian, L., and Winfree, E. (2011) Scaling Up Digital Circuit Computation with DNA Strand Displacement Cascades. *Science 332*, 1196−1201.
(37) Genot, A. J., Bath, J., and Turberfield, A. J. (2013) Combinatorial Displacement of DNA Strands: Application to Matrix Multiplication and Weighted Sums. *Angew. Chem., Int. Ed. 52*, 1189−1192.
(38) Zhang, D. Y., and Winfree, E. (2010) Robustness and modularity properties of a non-covalent DNA catalytic reaction. *Nucleic Acids Res. 38*, 4182−4197.
(39) Jiang, Y. S., Bhadra, S., Li, B., and Ellington, A. D. (2014) Mismatches Improve the Performance of Strand-Displacement Nucleic Acid Circuits. *Angew. Chem. 126*, 1876−1879.
(40) Yin, P., Choi, H. M., Calvert, C. R., and Pierce, N. A. (2008) Programming biomolecular self-assembly pathways. *Nature 451*, 318−322.
(41) Ducani, C., Kaul, C., Moche, M., Shih, W. M., and Hogberg, B. (2013) Enzymatic production of 'monoclonal stoichiometric' single-stranded DNA oligonucleotides. *Nat. Methods 10*, 647−652.
(42) Green, C., and Tibbetts, C. (1981) Reassociation rate limited displacement of DNA strands by branch migration. *Nucleic Acids Res. 9*, 1905−1918.
(43) Reynaldo, L. P., Vologodskii, A. V., Neri, B. P., and Lyamichev, V. I. (2000) The kinetics of oligonucleotide replacements1. *J. Mol. Biol. 297*, 511−520.
(44) Jose, D., Datta, K., Johnson, N. P., and von Hippel, P. H. (2009) Spectroscopic studies of position-specific DNA "breathing" fluctuations at replication forks and primer-template junctions. *Proc. Natl. Acad. Sci. U. S. A. 106*, 4231−4236.
(45) von Hippel, P. H., Johnson, N. P., and Marcus, A. H. (2013) Fifty years of DNA Breathing: Reflections on old and new approaches. *Biopolymers 99*, 923−954.
(46) Frank-Kamenetskii, M. D., and Prakash, S. (2014) Fluctuations in the DNA double helix: A critical review. *Physics of Life Reviews 11*, 153−170.
(47) Li, B., Jiang, Y., Chen, X., and Ellington, A. D. (2012) Probing Spatial Organization of DNA Strands Using Enzyme-Free Hairpin Assembly Circuits. *J. Am. Chem. Soc. 134*, 13918−13921.
(48) Tomov, T. E., Tsukanov, R., Liber, M., Masoud, R., Plavner, N., and Nir, E. (2013) Rational Design of DNA Motors: Fuel Optimization through Single-Molecule Fluorescence. *J. Am. Chem. Soc. 135*, 11935−11941.
(49) Thachuk, C., Winfree, E., and Soloveichik, D. (2015) Leakless DNA Strand Displacement Systems. *DNA Computing and Molecular Programming 9211*, 133−153.
(50) Machinek, R. R., Ouldridge, T. E., Haley, N. E., Bath, J., and Turberfield, A. J. (2014) Programmable energy landscapes for kinetic control of DNA strand displacement. *Nat. Commun. 5*, 5324.
(51) Chen, C. L., Wang, W. J., Wang, Z., Wei, F., and Zhao, X. S. (2007) Influence of secondary structure on kinetics and reaction mechanism of DNA hybridization. *Nucleic Acids Res. 35*, 2875−2884.
(52) Gao, Y., Wolf, L. K., and Georgiadis, R. M. (2006) Secondary structure effects on DNA hybridization kinetics: a solution versus surface comparison. *Nucleic Acids Res. 34*, 3370−3377.
(53) Zadeh, J. N., Steenberg, C. D., Bois, J. S., Wolfe, B. R., Pierce, M. B., Khan, A. R., Dirks, R. M., and Pierce, N. A. (2011) NUPACK: Analysis and Design of Nucleic Acid Systems. *J. Comput. Chem. 32*, 170−173.
(54) Bhadra, S., and Ellington, A. D. (2014) Design and application of cotranscriptional non-enzymatic RNA circuits and signal transducers. *Nucleic Acids Res. 42*, e58−e58.
(55) Puglisi, J. D., and Tinoco, I. (1989) [22] absorbance melting curves of RNA. *Methods in Enzymology 180*, 304−325.

NOTE ADDED AFTER ASAP PUBLICATION

The original version of this manuscript, published ASAP on March 2, 2016, contained data generated by the NUPACK web application at nupack.org. At the time the original calculations were performed, the NUPACK web application contained a bug in the implementation of the "dangles=all" case that affected the equilibrium pair probability prediction values. These values were used in availability and mutual availability calculations. The bug in the dangles=all option has since been corrected and the data in the present manuscript were calculated using the updated NUPACK code. The availability and mutual availability data and secondary structure plots in Figures 3 and 4 of the manuscript and Figures S3, S4, S5, S8, S9, S10, and S11 and Table S4 of the Supporting Information have been updated with the new calculations. The corrected version was reposted on November 1, 2016.

DOI: 10.1021/acssynbio.5b00231
ACS Synth. Biol. 2017, 6, 84−93